

# Giant photoinduced lattice distortion in oxygen-vacancy ordered **SrCoO<sub>2.5</sub> thin films**

Bingbing Zhang<sup>1</sup>, Jiali Zhao<sup>1</sup>, Huixia Fu<sup>2</sup>, Haidan Wen<sup>3</sup>, Can Yu<sup>1</sup>, Yujia Wang<sup>4</sup>, Nianpeng Lu<sup>4</sup>, Yuelin Li<sup>3</sup>, Sheng Meng<sup>2</sup>, Haizhong Guo<sup>5\*</sup> and Ye Tao<sup>1\*</sup>

<sup>1</sup>*Institute of High Energy Physics, Chinese Academy of Sciences, Beijing, 100049, China*

<sup>2</sup>*Institute of Physics, Chinese Academy of Sciences, Beijing, 100190, China*

<sup>3</sup>*Advanced Photon Source, Argonne National Laboratory, Argonne, Illinois, 60439, USA*

<sup>4</sup>*Department of Physics, Tsinghua University, Beijing, 100084, China*

<sup>5</sup>*School of Physical Engineering, Zhengzhou University, Zhengzhou, 450001, China*

\*Taoy@ihep.ac.cn

\*hguo@iphy.ac.cn

## Abstract

Despite of the tremendous studies of oxygen vacancy formation and migration in determining the structural evolution and property optimization of multivalent transition metal oxides, few has focused on the transient dynamic behaviors in the oxygen vacancy enrichment system under non-equilibrium states. In this work, we performed multi-timescale ultrafast X-ray diffraction techniques to monitor the structural dynamics in the oxygen-vacancy ordered  $\text{SrCoO}_{2.5}$  thin films and observed an unanticipatedly giant lattice distortion. Time-resolved synchrotron X-ray diffraction measurements were applied in the  $\text{SrCoO}_{2.5}$  thin films upon excitation of different photon energies for films with different thicknesses. The giant magnitude of photoinduced strain ( $\Delta c/c > 1\%$ ) and its distinct correlation with the pump photon energy indicate an undoubtedly non-thermal origin of the photoinduced strain. The sub-picosecond resolution X-ray diffraction reveals the formation and propagation of the coherent acoustic phonons and further elongates the maximum distortion in the magnitude by 1.4 times at early time points. We propose a plausible mechanism for the giant lattice distortion upon the 400-nm-laser photoexcitation that it is the  $p$ - $d$  charge transfer induced the rearrangement of the tilted Co-O octahedral induces the giant c-axis elongation.

Multivalent transition metal oxides (TMOs) have claimed serious attentions on basics of their intriguing physical properties and potential applications in energy technologies [1-4]. Since the static and dynamic behaviors of oxygen vacancies intrinsically control the functional flexibilities of TMOs including structural, magnetic, and electronic transport properties, many recent researches emerge to characterize the oxygen vacancy migration and structural evolution [5-7]. Among TMOs, the oxygen deficient  $\text{SrCoO}_x$  stands out as a prime candidate for studying the role of oxygen stoichiometry in determining its flexibility of physical behaviors due to the existence of two reversible topotactic phases [8-10]. The long-range ordering oxygen vacancies and rich polyhedral configurations make  $\text{SrCoO}_{2.5}$  more attractive not only on account of its high oxygen permeation capacity and anisotropic ionic conduction in practical application, but also as a model system to demonstrate oxygen vacancy related studies [11,12].

Besides the study of the intrinsic characteristics, physical and electrochemical properties manipulated by extrinsic conditions are also beneficial to the extending of potential applications. Various exotic properties resulting from the oxygen transport and phase transformations have been reported in  $\text{SrCoO}_{2.5}$  by prudent modification of the ambient condition including strain [13], pressure [14], voltage [15], and heat treatment [9,11], as well as the recently reported electric-field ionic liquid gating [16]. At atomic scale, the electric-induced oxygen vacancy formation and migration is observed by scanning transmission electron microscopy, revealing strong electro-chemo-mechanical coupling in  $\text{SrCoO}_{2.5}$  [7]. However, all these precursors are limited under equilibrium or metastable states, few studies have focused on the transient behaviors under nonequilibrium states. Photo-doping one system by a laser pulse provides a powerful method to interrogate the exotic transient phenomena e.g. superconductivity [17-19]. Ultrafast X-ray diffraction (UXRD) techniques have been widely used in different nanostructures of functionalities such as  $\text{Sr}_2\text{IrO}_4$  [20],  $\text{PbTiO}_3$  [21], and  $\text{BiFeO}_3$  [22,23], exemplifying its power in elucidating the relationship between the photoexcited carriers and the atomic-scale structural distortion under the nonequilibrium state.

In this letter, we present the synchrotron based UXRD measurements on the  $\text{SrCoO}_{2.5}$  thin films, precisely probing the ultrafast structural distortion as a function of time delay after the laser excitation of different photon energies. Both interband p-d transition and intraband d-d transition are achieved by applying different pump photon energies (1.55 eV and 3.1 eV). The ultrafast dynamics are monitored by observing the angular shift and peak broadening of the (008) Bragg diffraction. The giant out-of-plane strain ( $\Delta c/c > 1\%$ ) originating from the photoexcitation of 400-nm-laser pump is pronouncedly larger than that can be caused by the heat effect. Our sub-picosecond XRD measurements based on a laser-induced plasma X-ray source provide insight into the first 100 ps after excitation, precluding the temporal resolution limit of synchrotron X-ray pulse and revealing the emergence of an instantaneous strain and its acoustic-velocity limited propagation. The quantitative agreement of the peak shift evolution measured on both picosecond and femtosecond XRD setups indicate the same origin for the early and late time points. We propose that it is the photoexcited p-d charge transfer that drives the transient lattice distortion and its slow relaxation up to ns delays. The state modification induced by the photoexcited charge transfer couples strongly to the structure of the  $\text{SrCoO}_{2.5}$  unit cell, leading to the rearrangement of the twisted octahedral and tetrahedral. The unanticipatedly giant lattice distortion in the  $\text{SrCoO}_{2.5}$  film hence correlates to the existence of the ordered oxygen vacancies and shows trace of the relationship between the photoexcited carriers and the corresponding oxygen vacancy dynamics. On the other hand, comparing to the conventional irreversible heat effect, the reversible nonthermal strain monitored by optical pulses opens avenues to extend the promising manipulation of the cobalt oxides in structure, magnetism, and other exotic properties.

We studied the brownmillerite structure  $\text{SrCoO}_x$  for  $x=2.5$ , with alternating Co-O octahedral and tetrahedral layers stacked along the [001] direction and ordered oxygen vacancy channels arranged in the a-b plane, grown on (001)  $\text{LaAlO}_3$  substrates. The large band gap (6.2 eV) of the substrate guarantees the optical transparency for all the photon energies used in our measurements [24]. The direct

band gap ( $\sim 2.18$  eV) and Mott gap ( $\sim 0.45$  eV) of the  $\text{SrCoO}_{2.5}$  film have already been reported intensively [8,16] and can be derived from our optical absorption data (Fig. S1). Hence we can achieve the intraband d-d transition ( $\alpha$  peak $\sim 1.4$  eV) and the interband p-d transition ( $\beta$  peak $\sim 2.8$  eV), by tuning the pump photon energies (1.2, 1.55, 2.4, and 3.1 eV) of the laser pulses.

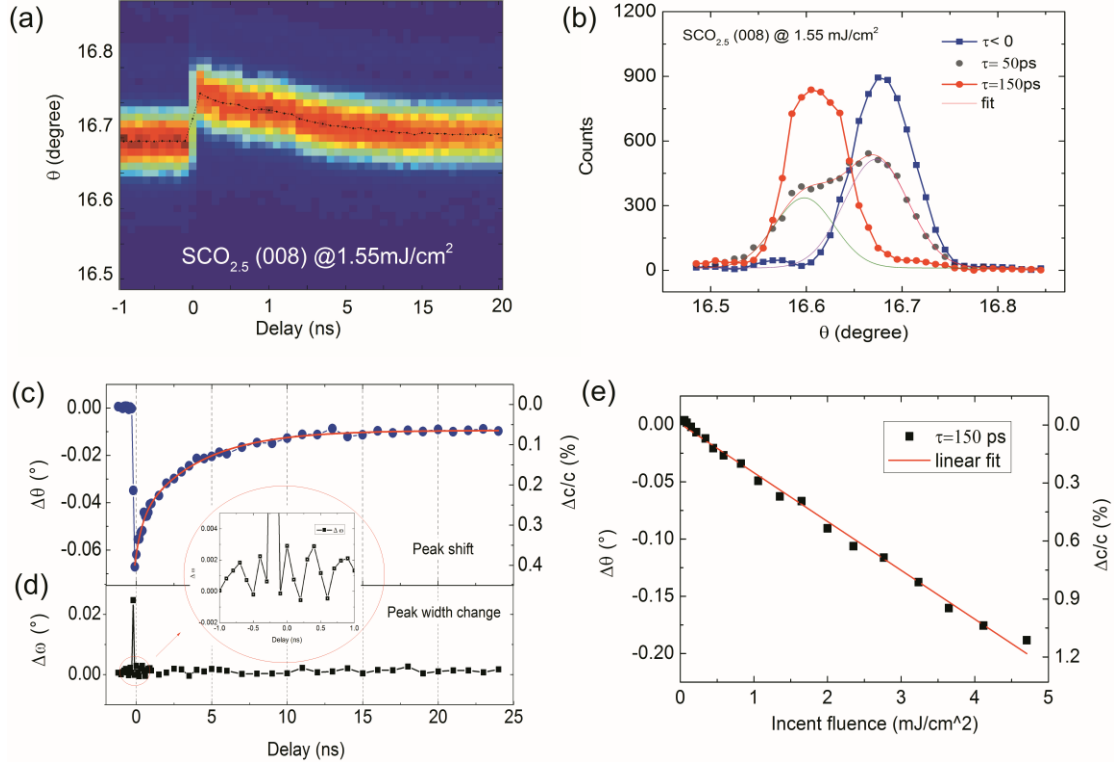


FIG. 1. (a) Time-resolved rocking curves of the  $\text{SrCoO}_{2.5}$  (008) Bragg peak as a function of time delay, after excitation of the 400-nm-laser pulses with incident fluence of  $1.55 \text{ mJ/cm}^2$ . The dotted points indicate the extracted peak center. (b) The  $\theta$ - $2\theta$  scans of the (008) reflection before ( $\tau < 0$ ), during ( $\tau = 50 \text{ ps}$ ), and after ( $\tau = 150 \text{ ps}$ ) the photoexcitation. The rocking curve at  $\tau = 50 \text{ ps}$  is fitted to a double-peak function. (c) The extracted peak shift and corresponding strain as a function of time delay from -1 to 24 ns, the data is empirically fitted to a biexponential decay function. (d) No peak width change or evolution can be found after photoexcitation. The exceptional point near zero delay corresponds to the superposition of the unexcited and excited parts, as shown in (b). The insert gives the enlarging of  $\Delta\omega$  near time zero. (e) Angular shift of (008) reflection and the induced strain at  $\tau = 150 \text{ ps}$  as a function of incident laser fluence from 0 to  $5 \text{ mJ/cm}^2$ , together with a linear fit to the data.

The time-resolved X-ray diffraction experiments upon photoexcitation of 1.55 eV (800 nm) and 3.1 eV (400 nm) were performed on a 43-nm-thick  $\text{SrCoO}_{2.5}$  film at 7-ID-C beamline of Advance Photon Source. The 400-nm pump pulses were generated by frequency doubling of the fundamental beam from a Ti:sapphire laser system, which was synchronized to the gated X-rays from the storage ring. The transient rocking curves shown in Fig. 1(a) were probed by X-ray pulses with photon energy of 11 keV after excitation of 400-nm-laser pulses. The penetration depth of 400-nm-laser in  $\text{SrCoO}_{2.5}$  is determined to be 30 nm, calculated from the optical spectra data. The angular shift to the smaller Bragg angle shown in Fig. 1(b) corresponds to an ultrafast out-of-plane expansion  $\Delta c/c = 0.404\%$  for the incident fluence of  $1.55 \text{ mJ/cm}^2$ . Note that the pump fluence in this manuscript all denotes the incident fluence without the calibration of optical absorption and reflectivity. Comparing with the previous  $\text{BiFeO}_3$  work (absorbed fluence  $\sim 3.2 \text{ mJ/cm}^2$ ,  $\Delta c/c = 0.41\%$  [23]), smaller than half of the fluence was needed to achieve the comparable strain level (absorbed fluence: 0.87 versus  $3.2 \text{ mJ/cm}^2$ ), manifesting the unusual lattice response in the  $\text{SrCoO}_{2.5}$  film. Furthermore, explicit linear fluence dependence of angular shift at  $\tau = 150 \text{ ps}$  was observed, indicating the possibility to achieve a much larger photoinduced strain ( $\Delta c/c > 1\%$ ) for a larger incident fluence of  $4.5 \text{ mJ/cm}^2$ , as shown in Fig. 1(d). As for fluence bigger than  $5 \text{ mJ/cm}^2$ , the strain reaches saturation together with apparent sample degradation.

The evolution of angular shift (Fig. 1(c)) and peak width change (Fig. 1(d)) of the  $\text{SrCoO}_{2.5}$  (008) reflection as a function of time are extracted from the time-resolved rocking curves in Fig. 1(a). The angular shift change can be well fitted to by a biexponential decay function with a fast time constant of 0.45 ns and a slow time constant of 4.3 ns. Unlike the giant change of the Bragg angle, the peak width of the reflection remains unchanged after photoexcitation, indicating a homogeneous spatial strain profile after the optical excitation (the insert figure within the red circle). The exceptional point around time zero does not refer to a photoinduced peak broadening but results from the temporal overlap of 40-fs laser and 100-ps X-ray pulses, when the diffracted X-ray pulses consist of the unexcited and excited regions

at the same time, as shown in Fig. 1(b).

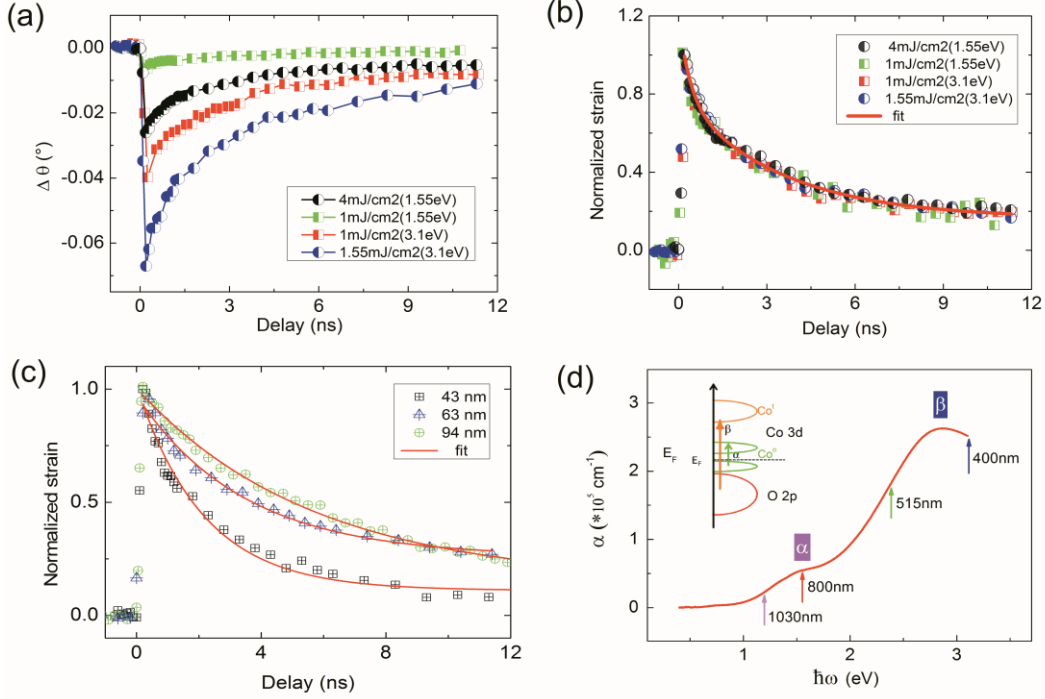


FIG. 2. (a) Angular shift of SrCoO<sub>2.5</sub> (008) reflection as a function of time delay at the different pump fluence and photon energies. (b) Normalized strain recoveries for the 45 nm sample at various pump conditions, the red solid line indicates a bioexponential decay fit. (c) Normalized photoinduced strain dynamics for 43-nm-thick, 63-nm-thick, and 94-nm-thick samples after photoexcitation. (d) Optical absorption of the SrCoO<sub>2.5</sub>/LaAlO<sub>3</sub> film with two characterized peak at 1.4 eV ( $\alpha$ ) and 2.8 eV ( $\beta$ ). Four pump wavelengths used in this work are also labeled with arrows. The inserted schematic shows the band diagram of SrCoO<sub>2.5</sub>, extracted from Ref [8].

The photoinduced strains at the various pump photon energies and incident fluence were also measured as a function of time delay, as shown in Fig. 2(a). It can be obviously seen, the angular shifts of the (008) Bragg peak excited by 800-nm (1.55 eV) pump pulse are much smaller than that by 400-nm (3.1 eV) pump pulse. Taking two 1 mJ/cm<sup>2</sup> cases for example quantitatively, the maximum angular shift at  $\tau = 150$  ps for the 3.1 eV case is about 6 times larger than that in 1.55 eV case with the same incident fluence, ascribing to two distinct photoexcited charge transfers, the intraband d-d transition ( $\alpha$  peak in Fig. 2(c)) and the interband p-d transition ( $\beta$  peak in Fig. 2(c)). However, the recoveries of the normalized strain for different fluence and pump

photon energies collapse into one curve for the 45-nm-thick sample, as shown in Fig. 2(b), reminiscent of the similar behavior in another Mott insulator  $\text{Sr}_2\text{IrO}_4$  [20]. The consistency decay behavior manifests a similar formalization and relaxation mechanism for the different pump fluence and photon energies induced strains. Both the p-d charge transfer and d-d transition will rapidly relax into the same configuration after photoexcitation via intraband relaxation such as carrier cooling or optical phonon emission ( $< 1$  ps). Broad consensus of the roles of photoinduced carrier emergence and relaxation in determining the buildup of the ultrafast strain ( $< 100$  ps) and the subsequent long-term decay (up to several tens of ns) have been already reached [20,23,25]. As shown in Fig. 2(d), strong thickness dependence of the strain recoveries was also observed in the  $\text{SrCoO}_{2.5}$  films, just as what happens in  $\text{Sr}_2\text{IrO}_4$  [20] and  $\text{BiFeO}_3$  films [26]. The characterized decay constant for the three samples are  $\tau = 2.14, 3.45$ , and  $7.0$  ns, respectively, and the thicker the sample is, the longer decay time occurs. The thickness dependent measurements were based on the high repetition rate UXRD setups implemented at 1W2B beamline of Beijing Synchrotron Radiation Facility, with photoexcitation of 19 kHz, 515 nm laser pulses.

The optical absorption spectrum of  $\text{SrCoO}_{2.5}$  is exhibited in Fig. 2(d) with two distinct peak features labeled as  $\alpha$  (1.4 eV) and  $\beta$  (2.8 eV). As reported in a previous work [8,16], peak  $\alpha$  is attributed to the *d-d* transition between two various Co 3d states and peak  $\beta$  to a *p-d* transition from O 2p state to Co 3d state, shown in the insert of Fig. 2(d). Therefore, by monitoring the wavelength of pump laser pulses (1030 nm, 800 nm, 515 nm, and 400 nm, marked with colorful arrows), we are able to employ measurements upon different photoexcited charge transitions. The excitation of 1030 nm and 800 nm laser pumps correspond to a *d-d* transition, while the 515 nm and 400 nm cases possibly give rise to the *p-d* charge transfer. On the other hand, the two band gaps of  $\text{SrCoO}_{2.5}$  can also be extracted from the given absorption spectra, as to be 0.45 eV for the Mott gap and 2.18 eV for the direct band gap, respectively (Fig. S1).

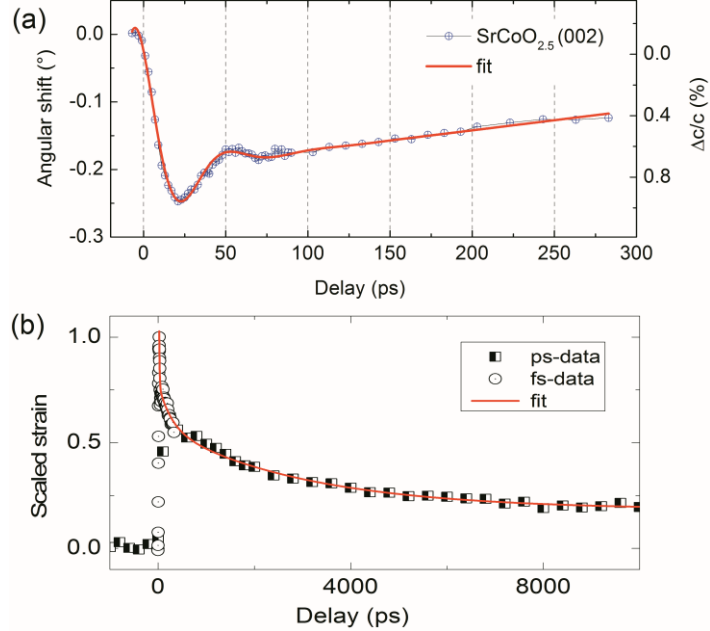


FIG. 3. (a) Transient angular shift and the corresponding photoinduced strain as a function of delay from -10 ps to 300 ps upon 800 nm laser pump at a fluence of 15 mJ/cm<sup>2</sup>. (b) The normalized peak shift of the (008) Bragg peak of the 94-nm-thick SrCoO<sub>2.5</sub> film, merging the fs-UXRD data (800 nm excitation) and the SR based ps-UXRD data (1030 nm); the magnitude of peak shifts were scaled considering the fluence difference between the two experimental. The red solid line refers to the fit to the merged data.

To overcome the temporal resolution limit of the SR X-ray pulses (~150 ps) and track the buildup of the photoinduced strain right after excitation, we performed the UXRD measurements on the 94-nm-thick SrCoO<sub>2.5</sub> film using a laser-based plasma X-ray source with sub-ps time resolution as complement, providing insight into the dynamics within the first 100 ps. Laser pulses with central wavelength of 800 nm were focused into a 780 μm (FWHM) spot to excite the sample. Fs X-ray pulses with photon energy of 8.047 keV are utilized to probe the lattice response within a 250 μm (FWHM) region. The photoinduced angular shifts, as well as the corresponding strain are shown in Fig. 3(a). Extraordinarily large strain of  $\Delta c/c \sim 1\%$  at  $\tau = 25$  ps was obtained when increasing the laser incident fluence to 15 mJ/cm<sup>2</sup>. No sample degeneration was observed during the measurement and no peak width change was observed. The scaled peak shift of the fs data collapses with the 1030 nm ps data, after ruling out their fluence deviations, as shown in Fig. 3(a), indicating the same

electronic origin of photoinduced strain at early and late time points. We also notice that the maximum photoinduced strain at  $\tau=25$  ps is about 1.4 times larger than that at 100 ps, which enlarge the possible lattice response that cannot be observed by the previous synchrotron UXRD measurements.

We interpret the evolution of the photoinduced strain presented in Fig. 3(b) as due to the propagation of coherent acoustic phonons, hence the extrusive oscillation feature around 50 ps is caused by the transmission of strain waves through the interface of film and substrate, resulting in a damping of the oscillation. The evolution of angular shift in Fig. 2(b) can be phenomenologically described by

$$\Delta\theta = A_1 e^{-t/\tau_1} + A_2 + A_3 e^{-t/\tau_0} \sin(2\pi t/T + \phi)$$

After subtracting the exponential decay background, the data can be well fitted using an oscillating decay-type function. The obtained attenuation period  $T=25 \pm 1$  ps corresponds to the time that strain front travels once across the film, indicating a strain pulse velocity of  $v = d/T = 94 \text{ nm}/25 \text{ ps} = 3.76 \text{ km/s}$ . The sound-speed limited strain dynamics within 100 ps implies an instantaneous stress upon photoexcitation in  $\text{SrCoO}_{2.5}$ .

So far, the multi-scale structural dynamics in the  $\text{SrCoO}_{2.5}$  film have been monitored in combination with fs and ps UXRD measurements, including the emergence and propagation of the photoinduced strain waves within the first 100 ps and the subsequent long-term relaxation process on ns time scale. As shown in Fig. 3(b), the merged strain recovery dynamics can be well fitted to a third order exponential decay function with decay constants as 23 ps, 2.4 ns, and 22 ns, corresponding to the strain wave, carrier recombination, and thermal effect, respectively. Although the evolution of the photoinduced strain has been well tracked, the origin of the instantaneous stress that induces the transient strain and the reason why such a giant lattice response happens still need further explanation.

First of all, one of the most widely known causes to the photoinduced expansion, the thermal contribution due to the above-band-gap excitation, must be excluded. The excess energy of the conduction band is transferred to the lattice through the

electron-phonon interaction and initiates the transient temperature jump. Therefore, the thermal contribution arising from the excitation of the different photon energies can be prudently estimated. Our calculation shows an identical amplitude of temperature jump excited by 400 nm laser pulses to 800 nm ones at the same fluence  $\Delta T_{400}/\Delta T_{800} \sim 1.01$ , which is far from explaining the actual large strain difference in quantity ( $\varepsilon_{400}/\varepsilon_{800} \sim 6$ ) between the two photon energies (see section II of support material). Furthermore, thermal expansion coefficient along out-of-plane direction for  $\text{SrCoO}_{2.5}$  is experimentally determined to be  $1.96 \times 10^{-5} \text{ K}^{-1}$  by the temperature varying XRD measurements (Fig. S2). We notice that only a rather huge temperature jump of 550 K can lead to an expansion of  $1.0 \times 10^{-3}$ , the same level as that can be obtained by 400 nm photoexcitation with a low incident fluence of  $4 \text{ mJ/cm}^2$  (Fig. 1(e)). Quantatively, we prudently calculated the temperature jump resulted from the photoexcitation of 400 nm laser pulses, considering the excess energy when the film was interband excited. The transient temperature increase was determined to be 30 K at a incident fluence of  $1.55 \text{ mJ/cm}^2$ , corresponding to an average expansion of  $\varepsilon = 30K \times 1.96 \times 10^{-5} \text{ K}^{-1} = 0.059\%$ , which only accounts for a small fraction of the actual photoinduced strain ( $\sim 0.059/0.404 = 14.6\%$ ), unambiguously revealing the nonthermal origin of the photoinduced strain upon 400 nm laser pump. However, for peak shift induced by 800-nm laser pulses, the estimated strain due to thermal contribution (0.058 %) perfectly matches the experimental data ( $\sim 0.06\%$ ), indicating a heat dominating photoinduced strain under this condition. Note that the Bragg peak intensity decreases sharply and the Bragg peak width exhibits an irreversible broadening during the heating treatment at high temperature (Fig. S2), indicating the unrecoverable degeneration of sample. However, the nonthermal strain monitored by the optical pulses provides an alternative method to manipulate the crystal structure at much higher levels without any degradation to the sample.

Apart from the thermal phonons of the excess energy ( $E_p - E_g$ ), the distribution changes of the excited electron-holes might also contribute to the stress, described as deformation potential [27]. However, this effect in our system can only lead to a

compressive stress due to the negative sign of  $dE_g/dP$  [14], contrary to our result. The ratio of transient stress arising from the deformation potential ( $\sigma^e$ ) to thermal effect

( $\sigma^p$ ) can be quantitatively calculated according to  $\frac{\sigma^e}{\sigma^p} = \frac{C}{3\beta} \frac{dE_g}{dP} \frac{1}{E - E_g}$  [27]. For an

interband p-d transition excited by the pump photon energy  $\sim 3.1$  eV, the ratio corresponds to a value of  $\sim -0.26$ , which indicates that the contribution of deformation potential effect is even smaller than the thermal contribution, but of the opposite sign. On all accounts, the overall stress due to the thermal contribution and the deformation potential interaction play no essential part in the transient lattice distortion.

On the other hand, the contribution due to the converse piezoelectric effect can also be ruled out because no proof of ferroelectricity in  $\text{SrCoO}_{2.5}$  has been reported. Generally, the magnitude of the photostriction depends on how large its structure can distort. The strength of covalent/ionic bonds thereby directly correlates to the lattice response that could be achieved. Comparing with the conventional perovskite-type structures, the presence of the ordered oxygen vacancies induce the intrinsic buckling of Co-O tetrahedral layers and the tilting of Co-O octahedron [28]. On the contrary, the formation and dynamics of oxygen vacancies will certainly deform the structure [5,7], indicating a strong coupling between oxygen stoichiometry variation and lattice spacing, as the defined chemical expansion [29]. The linear dependence between the electric field induced oxygen deficiency of  $\text{CoO}_x$  layers and the correlated lattice spacing have already been well investigated [6,7,30].

In this regard, we propose that it is the *p-d* charge transfer from the O  $2p$  to Co  $3d$  state in  $\text{SrCoO}_{2.5}$  that induces the giant *c*-axis elongation. Under the excitation of 400-nm laser pump, the state modification due to the *p-d* charge transfer induces the transient charge redistribution, manifested as reduction of the Co valence state and the concomitant charge increase of oxygen (could also be seen as decrease in oxygen stoichiometry or formation of oxygen vacancies) [31,32]. The strong coupling between oxygen deficiency and lattice spacing thereby leads to the rearrangements of the Co-O polyhedral layers, e.g. a rotation of the intrinsically tilted Co-O octahedral may happen and results in the giant extension of the interatomic spacing. Analogous

historical example of the photostriction occurs in the organic-inorganic lead halide perovskite sample  $\text{MAPbI}_3$ , where the weakening of the hydrogen bonding excited by charge transfer in turn relieves the buckling of the Pb-I octahedral, resulting in the lattice dilation [32]. The difference lies in the thing that couples to the tilted octahedral, it refers to the amine group in  $\text{MAPbI}_3$  whereas the oxygen vacancies in  $\text{SrCo}_{2.5}$ . Similarly, it is rational to assume that it is the weakening of the interaction between the oxygen vacancies and surrounding octahedral that brings the unanticipated giant lattice distortion in  $\text{SrCoO}_{2.5}$ . Note that the so called oxygen vacancy formation only corresponds to a minor change of the oxygen stoichiometry,  $\text{SrCoO}_x$  ( $x=2.46\sim2.5$ ) for a strain of 1.5 %, given the linear relation between the lattice spacing and the oxygen stoichiometry [7].

Our hypothesis can be supported by the several unintuitive characters of our measurements. First, for 800-nm laser photoexcitation, the  $d$ - $d$  charge transfer in the Co ions shows no net valence state changes and the corresponding oxygen vacancies formation, hence no noticeable structural distortion has been found. This can provide a notable explanation of the huge difference in the strain magnitude for excitation upon different photon energies (1.55 eV and 3.1 eV). Second, for the perovskite  $\text{SrCoO}_3$  sample, due to the absence of ordered oxygen vacancies and the corresponding octahedral tilt, the photoexcited lattice dilation arising from the  $p$ - $d$  transition should not be that large. Our UXRD measurement confirm the prediction, in comparison to the giant lattice response in  $\text{SrCoO}_{2.5}$ , only half of the photoinduced strain could be obtained in  $\text{SrCoO}_3$  upon 400-nm laser excitation at the same incident fluence, exemplifying the role of the oxygen vacancies in determining the giant lattice distortion. Furthermore, enlightened by the isotropic photoinduced response in  $\text{MAPbI}_3$  film, we prefer a spatial homogeneous stress profile in  $\text{SrCoO}_{2.5}$  as well, which can be further confirmed by the negligible peak width change of (008) reflection, as shown in Fig. 1(d).

Phenomenally, the photoexcited carriers strongly couple to  $\text{SrCoO}_{2.5}$  unit cell (including oxygen vacancy) and initiate an instantaneous stress, which will drive an ultrafast strain and the subsequent structural dynamics. The ultrafast buildup of the

photoinduced strain and its sound-limited evolution across the film can be resolved on basis of a laser-based fs X-ray source. The much slower ns scale recovery process is thereby tracked by SR-based measurements. The unanticipatedly giant photoinduced expansion upon the illumination of 400-nm-laser pulses can be viewed as the strong photo-chemo-mechanical coupling in the  $\text{SrCoO}_{2.5}$  films, manifested as photoexcited disorder transition (minor formation or migration) of the oxygen vacancies and the concomitant octahedral rearrangement. Our work provides deep insight into the role that the ordered oxygen vacancies play in multivalent transition-metal oxides and reveals traces of oxygen vacancies dynamics under non-equilibrium states. The manipulation of Co-O distortions or rotations via photoexcited carriers offers a promising route to tailoring the material properties and functionalities in a novel way. The studies of complicated and multiple timescale structural dynamics also call for the combination of ps and fs UXRD techniques.

## Reference

- [1] J. B. Goodenough, *Rep Prog Phys* **67**, 1915 (2004).
- [2] J. Suntivich, H. A. Gasteiger, N. Yabuuchi, H. Nakanishi, J. B. Goodenough, and Y. Shao-Horn, *Nat Chem* **3**, 546 (2011).
- [3] Z. P. Shao and S. M. Haile, *Nature* **431**, 170 (2004).
- [4] B. R. Wygant, K. A. Jarvis, W. D. Chemelewski, O. Mabayoje, H. Celio, and C. B. Mullins, *Acs Catal* **6**, 1122 (2016).
- [5] Y. M. Kim *et al.*, *Nat Mater* **11**, 888 (2012).
- [6] J. H. Jang *et al.*, *Acs Nano* **11**, 6942 (2017).
- [7] Q. H. Zhang *et al.*, *Nat Commun* **8** (2017).
- [8] W. S. Choi, H. Jeen, J. H. Lee, S. S. A. Seo, V. R. Cooper, K. M. Rabe, and H. N. Lee, *Phys Rev Lett* **111** (2013).
- [9] H. Jeen *et al.*, *Nat Mater* **12**, 1057 (2013).
- [10] Q. Y. Lu, Y. Chen, H. Bluhm, and B. Yildiz, *J Phys Chem C* **120**, 24148 (2016).
- [11] H. Jeen, W. S. Choi, J. W. Freeland, H. Ohta, C. U. Jung, and H. N. Lee, *Adv Mater* **25**, 3651 (2013).
- [12] R. Le Toquin, W. Paulus, A. Cousson, C. Prestipino, and C. Lamberti, *J Am Chem Soc* **128**, 13161 (2006).
- [13] S. J. Callori *et al.*, *Phys Rev B* **91** (2015).
- [14] F. Hong, B. B. Yue, Z. X. Liu, B. Chen, and H. K. Mao, *Phys Rev B* **95** (2017).
- [15] Q. Y. Lu and B. Yildiz, *Nano Lett* **16**, 1186 (2016).
- [16] N. P. Lu *et al.*, *Nature* **546**, 124 (2017).
- [17] M. Mitrano *et al.*, *Nature* **530**, 461 (2016).
- [18] R. Mankowsky *et al.*, *Nature* **516**, 71 (2014).
- [19] D. Fausti *et al.*, *Science* **331**, 189 (2011).
- [20] Y. L. Li, R. D. Schaller, M. Z. Zhu, D. A. Walko, J. Kim, X. L. Ke, L. D. Miao, and Z. Q. Mao, *Sci Rep-Uk* **6** (2016).
- [21] D. Daranciang *et al.*, *Phys Rev Lett* **108** (2012).
- [22] D. Schick *et al.*, *Physical Review Letters* **112**, 097602 (2014).
- [23] H. D. Wen *et al.*, *Phys Rev Lett* **110** (2013).
- [24] N. Goel *et al.*, *Appl Phys Lett* **91** (2007).
- [25] D. Schick *et al.*, *Phys Rev Lett* **112** (2014).
- [26] Y. L. Li *et al.*, *Sci Rep-Uk* **5** (2015).
- [27] C. Thomsen, H. T. Grahn, H. J. Maris, and J. Tauc, *Phys Rev B* **34**, 4129 (1986).
- [28] T. G. Parsons, H. D'Hondt, J. Hadermann, and M. A. Hayward, *Chem Mater* **21**, 5527 (2009).
- [29] S. B. Adler, *J Am Ceram Soc* **84**, 2117 (2001).
- [30] X. Y. Chen, J. S. Yu, and S. B. Adler, *Chem Mater* **17**, 4537 (2005).
- [31] N. Gedik, D. S. Yang, G. Logvenov, I. Bozovic, and A. H. Zewail, *Science* **316**, 425 (2007).
- [32] Y. Zhou *et al.*, *Nat Commun* **7** (2016).

## Support materials

### I. Two band gap of $\text{SrCoO}_{2.5}$ film arising from the optical spectrum

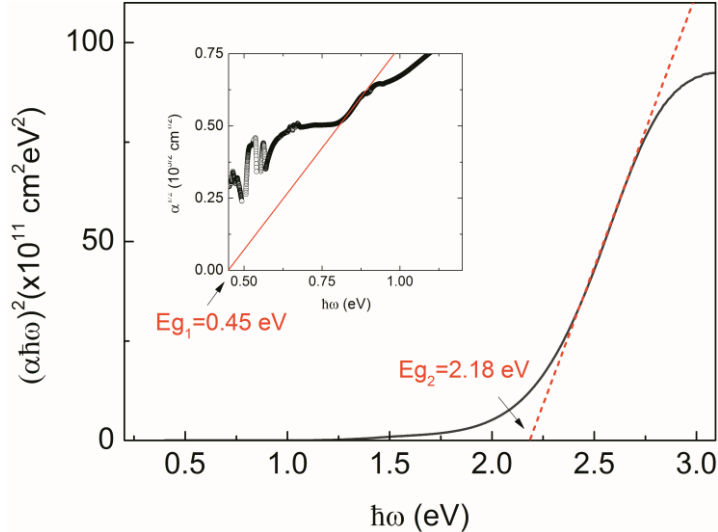


FIG. S1.  $(\alpha\hbar\omega)^2$  and  $\alpha^{1/2}$  (the inset) versus  $\hbar\omega$  plots of absorption spectra to obtain the two band gaps of  $\text{SrCoO}_{2.5}$ , as Mott gap  $Eg_1 \sim 0.45$  eV and the direct band gap  $Eg_2$  corresponds to  $\sim 2.18$  eV, respectively.

### II. Analyses of photoinduced thermal contribution

#### a. Calculation of transient temperature jump

The transient temperature jump resulting from the excess energy of the conduction band can be calculated according to

$$\Delta T = \frac{F_{abs}(E_p - E_g)}{c_p \rho D E_p}$$

$$F_{abs} = F_p (1 - R) [1 - e^{(-\frac{\alpha D}{\cos\theta})}]$$

with parameters shown in the following Tab. S1

|                              |        |      |                  |
|------------------------------|--------|------|------------------|
| Incident laser fluence $F_p$ |        | 1.55 | $\text{mJ/cm}^2$ |
| Reflectivity $R$             | 400nm  | 0.22 | N.A.             |
|                              | 800 nm | 0.1  |                  |
| Film thickness $D$           |        | 43   | nm               |

|                                       |        |                       |                   |
|---------------------------------------|--------|-----------------------|-------------------|
| Absorption coefficient $\alpha$       | 400 nm | 0.033                 | nm <sup>-1</sup>  |
|                                       | 800 nm | 0.01                  |                   |
| Mott band gap $E_{g1}$                |        | 0.45                  | eV                |
| Direct band gap $E_{g2}$              |        | 2.18                  |                   |
| Laser incident angle $\theta$         |        | 45                    | degree            |
| Density $\rho$                        |        | 5.2                   | g/cm <sup>3</sup> |
| Thermal expansion coefficient $\beta$ |        | 1.96*10 <sup>-5</sup> | K <sup>-1</sup>   |
| Specific heat per unit mass $c$       |        | 0.5                   | J/(g*K)           |

Therefore, the ratio of temperature jump arising from 400 nm pump to that of 800 nm pump is determined by using the parameters listed in Tab. S1 as

$$\Delta T_{400nm} / \Delta T_{800nm} = \frac{(1-R_{400})[1-e^{(-\frac{\alpha_{400}D}{\cos\theta})}](E_{p1}-E_{g1})E_{p2}}{(1-R_{800})[1-e^{(-\frac{\alpha_{800}D}{\cos\theta})}](E_{p2}-E_{g2})E_{p1}} = 1.01$$

with an almost same amplitude, which obviously cannot explain the rather huge strain difference between different pump photon energies. In fact, we obtain a quantitative temperature jump of  $\sim 30$  K for the fluence of 1.55 mJ/cm<sup>2</sup>. In combination of the measured thermal expansion coefficient (Fig. S2), a thermal induced strain is estimated as to be 0.059%, which is far from the actual strain of 0.404% in our UXRD measurement upon 400 nm pump whereas consistent with that observed in 800 nm cases  $\sim 0.06\%$ . Hence, we propose that the thermal contribution play important role in determining the photoinduced strain excited by 800 nm laser pulses but not a crucial part in the 400 nm case.

### b. Temperature-varying XRD measurements

We performed the temperature-varying XRD experiments on SrCoO<sub>2.5</sub>/LaAlO<sub>3</sub> sample from room temperature to 650 °C by measuring the Bragg peak shift of SrCoO<sub>2.5</sub> (008) and LaAlO<sub>3</sub> (002) reflections, as shown in Fig. S2. The measurements performed at X-ray Diffraction Beamline of Shanghai Synchrotron Radiation Facility give a linear expansion coefficient of the film as 1.96\*10<sup>-5</sup> K<sup>-1</sup>.

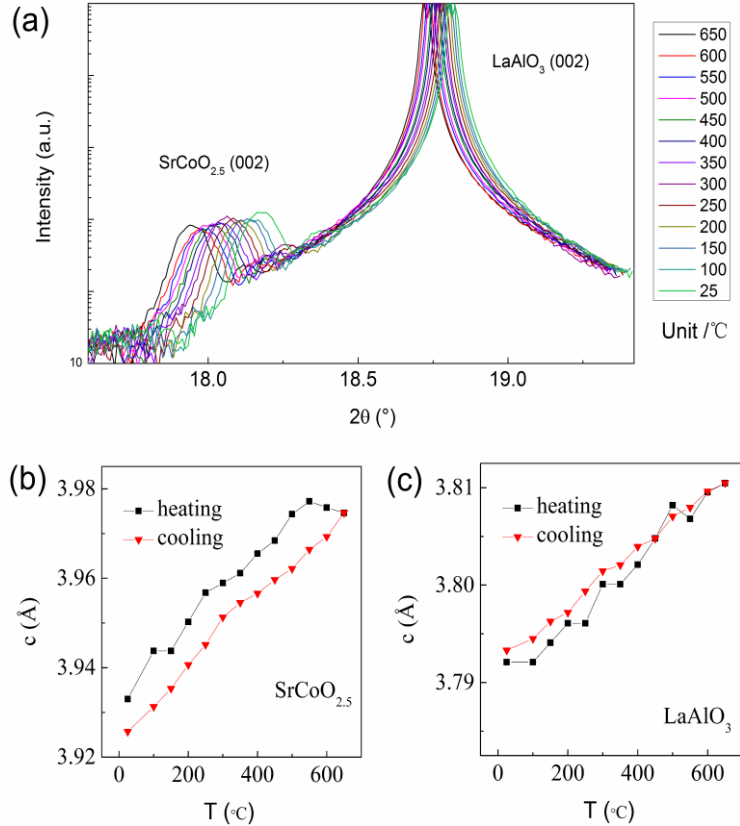


FIG. S2. a Temperature varying XRD results on (008) Bragg peak of film and the substrate from 25 to 650  $^{\circ}$ C, measured with SR pulses with photon energy of 18 keV. The corresponding crystal parameters of SrCoO<sub>2.5</sub> layer (b) and LaAlO<sub>3</sub> substrate (c) was obtained during heating (black) and cooling (red) processes.

### c. Estimation of the deformation potential effect

Upon laser illumination, photoexcited changes of electron and phonon distribution functions will couple to the structure and induce a stress. Thereinto, the electron-hole contribution to the stress refers to the deformation potential effect as

$\sigma_{ij}^e = -B \frac{dE_g}{dP} \delta_{ij} \delta n_e$ , while the thermal phonons of the excess energy contribute to the

stress as  $\sigma_{ij}^p = -\frac{3B\beta}{C} (E_p - E_g) \delta_{ij} \delta n_e$ . Therefore, we can obtain the ratio of these two contributions to the overall stress as

$$\frac{\sigma^e}{\sigma^p} = \frac{C}{3\beta} \frac{dE_g}{dP} \frac{1}{E_p - E_g}$$

where C is specific heat per unit volume and  $\beta$  is the linear expansion. The ratio is determined to be  $\sim -0.25$  for 400 nm photoexcitation, as a subtraction from the

thermal phonon strain, given the negative correlation of the band gap to pressure  $\sim 0.04$  eV/GPa [1]. The compressive stress due to the deformation potential effect tends to be compensation to the entire expansion.

### III. Photoinduced strain in $\text{SrCoO}_3$ film

We meant to measure the evolution of (002) Bragg peak of a 45 nm thick  $\text{SrCoO}_3$  film as a function of time delay with the same incident fluence. However, an evident irreversible transition occurs while implying 400 nm laser pulses onto the sample, characterized as a fluence-dependent drift of the static (002) reflection. In our opinion, the irreversible peak drift might be ascribed to a photoexcited phase transition from  $\text{SrCoO}_3$  to  $\text{SrCoO}_{2.5}$ . Thus, the overall photoinduced strain consists of two components: the irreversible static peak drift and the reversible transient peak shift. By fixing the time delay at  $\tau = 100$  ps, we measure the overall peak shift and the static peak drift as a function of pump fluence for 400 nm illumination, as shown in Fig. S3. After subtraction of the irreversible transition, the photoinduced strain arising from p-d charge transfer is determined to be 0.126% for a fluence of 1 mJ/cm<sup>2</sup>, only accounting for half of the strain magnitude in  $\text{SrCoO}_{2.5}$  case (0.258%) at same experimental condition.

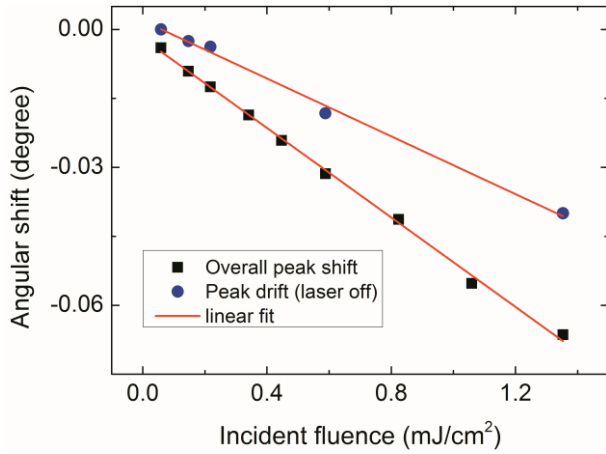


FIG. S3. The overall peak shift (black squares) of (002) reflection of  $\text{SrCoO}_3$  thin film upon 400 nm laser pump as a function of incident fluence. The blue circles indicate the Bragg peak drift at the respective fluence (shifts of laser-off peak center).